Wound-Induced Syncytia Outpace Mononucleate Neighbors during *Drosophila* Wound Repair

James S. White[1,2], Jasmine J. Su[1,4], Elizabeth M. Ruark[1], Junmin Hua[1], M. Shane Hutson[3,4,5,*], Andrea Page-McCaw[1,2,6,7,*]

***Correspondence:**

andrea.page-mccaw@vanderbilt.edu

shane.hutson@vanderbilt.Edu

Author contributions: Conceptualization, J.S.W., A.P.M., M.S.H.; Formal Analysis, J.S.W., J.J.S.; Investigation, J.S.W., J.J.S., E.M.R., J.H.; Writing – Original Draft., J.S.W., A.P.M.; Visualization, J.S.W., J.J.S.; Supervision, A.P.M., M.S.H., J.S.W. ; Project Administration, J.S.W., A.P.M., M.S.H; Funding Acquisition, A.P.M., M.S.H

[1]Dept. Cell and Developmental Biology, Vanderbilt School of Medicine, Nashville, TN; [2]Program in Developmental Biology, Vanderbilt University Nashville, TN; [3]Dept. Physics and Astronomy Vanderbilt University Nashville, TN; [4]Dept. Biological Sciences, Vanderbilt University, Nashville, TN; [5]Institute for Integrative Biosystems Research and Education, Vanderbilt University, Nashville, TN; [6]Vanderbilt-Ingram Cancer Center, Vanderbilt University, Nashville, TN; [7]Lead Contact; *Corresponding Authors

SUMMARY:

Injury is a constant reality of life, and survival requires all organisms to repair wounds. Cell behaviors like proliferation, migration, and invasion replace missing cells and close wounds [1, 2]. However, the contribution of other wound-induced cell behaviors is not understood, including formation of multi-nucleate syncytia. Wound-induced epithelial syncytia were first reported around epidermal puncture wounds in Drosophila larvae and adults [3, 4] with similarities to multinucleation increases in mammalian cardiomyocytes after pressure overload [5]. Although these tissues are post-mitotic, syncytia have more recently been reported in mitotically competent tissues: around laser wounds in Drosophila pupal epidermis and in zebrafish epicardium damaged by endotoxin, microdissection, or laser [1]. Further, injury induces fusion of other cells: after injury, bone marrow derived cells fuse with various somatic cells to promote repair [6-9], and after biomaterial implantation, immune cells fuse into multinucleated giant cells associated with rejection [10]. These observations raise the possibility that syncytia offer adaptive benefits, but it is unknown what those benefits are. Here, we utilize *in vivo* live imaging to analyze wound-induced syncytia in mitotically competent *Drosophila* pupae. Almost half the epithelial cells near a wound fuse, forming large syncytia. Syncytia migrate rapidly, outpacing diploid cells to complete wound closure. We show syncytia can both pool resources of their component cells to concentrate them toward the wound, and reduce cell intercalation during wound closure, two mechanisms for speeding wound repair. In addition to wound healing, these properties of syncytia are likely to contribute to their roles in development and pathology.

RESULTS:

A mitotic tissue utilizes cell-cell fusions during wound repair.

The pupal notum is a mono-layer columnar epithelium composed of diploid cells that undergo regular mitotic cycles [11] (Fig. S1A-C). To analyze cell behaviors around wounds, we live-imaged after laser ablation, labeling cell borders with p120ctnRFP [12] and nuclei with His2GFP. Two hours after wounding, we observed prominent multinucleate syncytial cells around the wound (Fig.1A, Movie S1). Some syncytia appeared to contain over a dozen nuclei, but because of the non-prismatic nature of notum epithelial cells, nuclei rarely aligned with apical borders in a 2-D projection (Fig. S1D). We estimated the number of nuclei within the largest syncytia based on apical area and nuclear density: 1 h after wounding the three largest syncytia contained on average 3-13 nuclei, and 2 h after wounding they nearly doubled to 6-20 nuclei (Fig. 1B). Interestingly, larger wounds generated syncytia with larger apical areas and more nuclei, proportional to wound size, suggesting syncytium formation is a dynamic and scalable response to injury (Fig. 1 C-E).

Imaging cell borders after wounding revealed the gradual loss of p120ctn between some epithelial cells followed by syncytial rounding (Fig.1F), suggesting cell fusion. As p120ctn was lost, E-cadherin-GFP was also lost (Fig. S1F-H), a phenomenon we call “border breakdown”. Border breakdowns were found spatially clustered in the first three to four rows of cells, 30-50 μm from the leading edge, and they occurred primarily within the first hour after wounding, some within 10 minutes after wounding (Fig 1G,H). To confirm border breakdowns were truly fusions, we analyzed cytoplasmic mixing. Individual GFP-labeled cells were generated at random locations. Before wounding, the level of cytoplasmic GFP fluorescence was stable yet exhibited cell-to-cell variability, allowing some differentiation of cells by intensity. Minutes after

a nearby laser ablation, GFP frequently diffused from labeled cells into neighboring unlabeled cells, followed later by loss of the corresponding border (Fig 1I, Movie S2). Border breakdowns between labeled and unlabeled cells were always preceded by GFP mixing (n=11). Thus, epithelial fusion is a rapid local response to wounding.

Cell shrinking is a second form of cell-cell fusion occurring later during wound closure.

Because border breakdowns occurred mostly within one hour after wounding, it was unclear how syncytia grew 1-2 h after wounding. However, an unexpected cell behavior was frequently observed: the apical area of diploid cells shrank until they disappeared, termed 'shrinking cells' (Fig. 2A). To determine if shrinking cells were extruding, we tracked a shrinking cell's nucleus (Fig. 2B). However, rather than extruding basally, the nucleus moved laterally to join a neighboring syncytium (n=7), suggesting fusion. Shrinking cells were distributed similarly around wounds as border breakdowns but were more numerous (Fig. 2C,D). To better understand this behavior, we analyzed individual GFP-labeled cells. Using cytoplasmic GFP or actin-GFP, we identified two classes of shrinking cells: many contributed GFP to a neighboring cell before they shrank (66%, Fig. 2E, Movie S3) indicating cell fusion; fewer appeared to lose GFP as they shrank (34%, Fig. 2F) indicating death. Thus, fusion can appear as border breakdown or cell shrinking. To determine the probability of fusion, we analyzed over 100 randomly-labeled single GFP cells within the radius of observed fusion (80 µm) and tracked them for 6.5 h to assess their fate. We found that a full quarter of the cells fused by either method (25%), 7.5% died, and 67% persisted as diploid cells with stable GFP. Fusing cells were strongly skewed toward the center of the wound: within 70 µm, about half the cells underwent fusion (47%), 11% died, and 42% persisted (Fig. 2G^{i}-G^{ii}). Although ~1/3 of shrinking cells die

(lose their GFP-labeled cytoplasm), shrinking-death is confined to the first 140 min whereas shrinking-fusion continues for over 300 min after wounding (Fig. S2A,B). Shrinking-fusion accounts for more than half of fusing cells (Fig. 2G^{iii}). The spatial distribution of fusing cells that shrank vs. lost borders was similar (Fig. 2E^{iii}), but compared to border breakdowns, shrinking initiation was delayed, continued for several hours after wounding (Figs. 2D, S2B), and took longer to complete (Fig. S2C). Thus, shrinking fusion accounted for continuing syncytial growth after border breakdowns subsided. Further, cell fusion is a persistent behavior over the course of wound closure.

Syncytia outcompete mononucleate cells at the leading edge of repair.

GFP labeling revealed that syncytia frequently overtook unfused cells as they moved toward the wound (Fig. 3A). Even without GFP-labeling, large syncytia were observed to push out smaller cells from the leading edge (Fig. 2B-C). The leading edge lacks adherens junctions and p120ctnRFP but is visualized clearly with MyoIIGFP/Zip-GFP, which we used to analyze the persistence of mononuclear and syncytia cells at the leading edge over the course of wound closure (Fig. 3 D-F). ~30 min after wounding, the leading edge formed from 10-13 small cells in addition to some syncytia; however, as the wound closed the syncytia became larger and displaced the small cells, with the last small cell removed from the leading edge well before closure 20-160 min later (Fig. 3 D-F). When the leading edge formed, syncytia occupied ~75% of the perimeter, but they took over the entire perimeter by 120-180 min (Fig. 3G). No small cell persisted at the leading edge through wound closure, suggesting syncytia are better able to re-epithelize wounds than diploid cells.

Syncytia move actin to the wound and eliminate intercalation.

How does fusion contribute to wound closure? Fusion may occur between adjacent cells equidistant from the wound (radial border fusion), producing a syncytium elongated along the wound edge, or fusion may occur between adjacent cells at different distances from the wound (tangential border fusion), producing a spoke-like syncytium pointing into the wound (Fig. 4A). These orientations might provide different benefits for wound repair: radial border fusions could reduce the requirement for cell intercalation, known to be a rate-limiting step of wound repair [13], whereas tangential border fusions might provide a way for cellular resources in distal cells to move toward the wound to contribute to closure. Although assessing the axis of fusion is difficult in shrinking cells, border breakdowns were readily binned as radial or tangential. In four wounds, 235 such events were identified; they were similarly distributed around the wound (Fig. S3A), yet more tangential borders broke down than radial borders (196 vs 39) and the bulk of them broke down sooner (Fig 4B).

To determine if spoke-like cells generated by tangential border breakdown transported resources to the leading edge, we generated individual cells expressing Actin-GFP and wounded such that unlabeled cells intervened between the labeled cell and the leading edge (Fig 4C). On fusion, actin-GFP flowed from the labeled cell to unlabeled neighbors. Strikingly, Actin-GFP always moved toward the wound (n=14). Although for ~1/3 of the labeled cells, actin-GFP moved both toward and away from the wound, actin-GFP never moved only away from it (Fig. 4C). In some of these cases (n=7), actin-GFP moved through several cells to aggregate at the leading edge (Fig. 4 D,E, Movie S4). Thus, cell fusion is a novel mechanism that allows transport to the leading edge of actin and perhaps other resources that would otherwise be trapped in distal cells. Increased actin at the front of syncytia would speed both their migration

and constriction of the actin cable around the wound compared to diploid cells. To consider the contribution of radial border fusions to wound closure, we analyzed the three wounds from Fig 3D-G and asked how many leading edge cells fused radially vs. intercalated: 16-41% of cells removed from the leading edge were removed through fusion, reducing the burden of intercalation substantially (Fig. 4F). Interestingly, the more the burden of intercalation was reduced, the faster the wound closed (Fig. 4G). Thus, syncytia formed by fusions of both radial and tangential borders are especially well suited to closing wounds.

DISCUSSION:

Previous work established that polyploid cells are important for closing epithelial wounds in post-mitotic tissues [4]. Here we report that syncytia have specific properties that aid wound repair in an otherwise diploid tissue. Live imaging demonstrates that syncytia advance toward the wound faster than smaller cells, pushing them out to form a wound margin eventually composed entirely of syncytia. Their speed derives in part from their ability to pool resources from a large area and concentrate them subcellularly where needed. We demonstrated syncytial resource pooling by imaging post-wound single cells expressing Actin-GFP. Actin synthesized in a distal cell moves toward the wound through cells fused along borders tangential to the wound; we observed actin to cross through four cells to arrive at the wound margin. Actin promotes migration by protruding membranes, and it promotes closure by encircling the wound with a thick constricting actin cable. Syncytial resource pooling is a generalizable phenomenon that could include other cytoskeletal proteins and organelles such as mitochondria and ribosomes. In addition to targeting resources to the wound margin, fusion of tangential borders may allow heavily damaged cells near wounds to survive through contributions from less damaged distal neighbors. Fusion of radial borders presents another advantage: by fusing, syncytia eliminate some cell intercalations at wound closure, thus speeding the slowest step of wound repair [13].

In the pupal notum, like in fly larval and adult epidermis, wound-induced syncytia form by fusion of epithelial cells [4, 14]. We estimate that within 70 µm of the wound center, containing about 5 rows of surviving cells, more than half the diploid cells fuse to form syncytia. Live imaging of GFP-labeled cells shows that cells start fusing within minutes after wounding and continue for several hours, enlarging syncytia. We observed two distinct forms of fusion: some cells break down their apical borders over 20 minutes, whereas others appear to shrink

their apical surface over the course of about an hour; shrinking cells must have fusion pores in basolateral membranes whereas border-breakdown fusion pores may be nearer apical adherens junctions. In addition to fusion pore positioning, border breakdowns and shrinking have distinct timings, with shrinking fusion occurring for hours after wounding and likely accounting for the continuing enlargement of syncytia. These differences suggest differences in the initiation of the two types of fusion, with shrinking cell timing consistent with larval autophagy-driven fusion [14], but we have no evidence the resulting syncytia have different properties. Interestingly, syncytial size is proportional to wound area; it is unclear how the syncytia can estimate wound size.

Our findings on syncytia pooling resources and reducing intercalation to increase migration and wound closure are likely to be relevant for syncytia arising in other contexts. Cell fusion is widely observed throughout development in both vertebrates and invertebrates: for example myoblasts fuse into muscles [15, 16], and fusion occurs in the *C. elegans* hypodermis [17] and vertebrate trophoblast [18], and osteoclast [19] lineages. Pathogen-induced epithelial fusion allows spreading of many viruses [20], and the fusion of cancer cells with bone-marrow derived cells is implicated in metastasis [21]. Tumor cell fusions form syncytial polyploid giant cancer cells in response to chemotherapeutics [22-25] and they exhibit increased migration and invasion potential [26, 27] escape further treatments due to increased resistance to genotoxic stress [28]. Thus in both polyploid giant cancer cells and wound-induced syncytia, stress-induced cell fusion leads to migratory advantages. These parallels highlight the importance of gaining a basic understanding of how induced syncytial cells form and function.

FIGURE LEGENDS:

Figure 1. Syncytia are induced by wounds.

A) Syncytia forming within 2 hr post wounding. **B)** Estimated nuclei per syncytium, mean SD. **C-D)** Syncytia scale with wound size, 3 hr post wounding, single syncytium outlined. **E)** Apical area of three largest syncytia is proportional to initial wound size, mean SD. **F)** Apical borders are lost (white arrowhead) as syncytia form. Original cells are numbered. **G)** Lost borders (white) mapped to first frame after wounding. Darkened cells will die, leading edge will form at dashed line. **H)** Distance and time of all border breakdowns in 3 wounds, leading-edge locations indicated. **I)** GFP from cell 1 mixes with neighboring cells 2-4 by 2 min after wounding, followed by visible border breakdown (white arrow). Maximum intensity projections in A, C-D, G; single Z slices in F, I. Scales: A-D, G = 20 µm, F,I = 10 µm.

Figure 2: Many cells near the wound fuse.

A-B) Cell (yellow arrow) shrinks from the epithelium after wounding (A). Its nucleus (asterisk) enters a neighboring syncytium, outlined in B^{iv}. Other shrinking cells are visible in A. **C)** All shrinking cells mapped to first frame after wounding. **D)** All shrinking cells and border breakdowns were tracked in 4 wounds. **E)** After wounding, cell 1 fuses with cells 2-6 evidenced by Actin-GFP sharing, then cell 1 shrinks from the epithelium. **F)** After wounding, cell 1 loses cytoplasmic GFP then shrinks, interpreted as death. **G)** GFP labeled cells in the region of fusion (80 µm) were tracked for 6.5 hr around 5 wounds to determine frequency of persistence (no GFP mixing), fusion (GFP mixing), or death (GFP loss). Fusion is common within 70 µm. Shrinking-fusion and border-breakdown fusion occur at similar locations (G^{iii}). Images are maximum intensity projections in A-B, single Z slices in E-F. Scale = 10 µm.

Figure 3: Syncytia outpace smaller cells

A) Before wounding, two clones are labeled with GFP, 1-2 and 3-4 (white numbers). After wounding, cells 2 and 3 fuse with neighbors 5-9 to form a syncytium (dashed leading edge in Aiii), which advances toward the wound, passing unfused cell 4 (arrow). **B-C)** Unfused cell (outlined) with corresponding nucleus (asterisk) is replaced at leading edge by neighboring syncytia (S, yellow arrows). **D)** Small cells are excluded from leading edge well before wound closure. **E,F)** Many unfused cells (arrows) occupy leading edge 30 min after wounding. At 120 min, the last unfused cell is ejected from leading edge (arrow). The wound closed at 190 min. **G)** Percent of leading-edge perimeter occupied by syncytia increases to 100%. Images are single Z slices in A^{i}-A^{ii} and maximum intensity projections in A^{iii}-F. Scale: A,E-F = 20 µm, B-C = 10 µm.

Figure 4: Cell fusions are beneficial for wound closure.

A) Illustration of tangential vs radial border breakdown. **B)** More tangential than radial borders break down after wounding. **C)** Individual actin-GFP labeled cells demonstrate actin is directed toward the wound through syncytia. **D-E)** Before wounding, actin-GFP in cell 1 is three cells away from the future leading edge. After wounding, fusion of cells 1-4 allows actin-GFP to move to the leading-edge actin cable. Single Z slices for pre-wound and 2 min; maximum intensity projections for 10-30 min. Scale = 10 µm. **F)** Radial border fusion can reduce intercalation at a wound. **G)** Intercalations and fusions around the wounds of Fig. 3D,G.

Supplemental Movie 1: Syncytial cells form after wounding in the Drosophila pupal notum.

Cell borders in red (p120ctnRFP) and nuclei in green (HistoneGFP).

Supplemental Movie 2: GFP mixing precedes border breakdown after wounding. Arrow in first frame points to cell border between cells that will fuse after wounding. GFP diffusion into the unlabeled cell precedes visible border breakdown. w, wound region. Cell borders are labeled with P120ctnRFP.

Supplemental Movie 3: Shrinking cells contribute to syncytia. Arrow in first frame points to an individual cell that fuses after wounding, first contributing its actin-GFP to neighboring cells and then shrinking from the apical plane. w, wound region. Cell borders are labeled with P120ctnRFP.

Supplemental Movie 4: Syncytia pool actin at the leading edge of repair. An individual cell labeled with actin-GFP fuses with wound proximal cells and contributes its actin to the leading edge of the syncytium. w, wound region. Cell borders are labeled with P120ctnRFP.

Acknowledgements: We thank James O'Connor for his original observations of syncytial cells around pupal wounds, and Kimi LaFever Hodge for technical assistance. We thank the BDRC for fly stocks. J.S.W. was supported by T32HD007502. This work was supported by the National Institute of General Medical Sciences R01GM130130 to APM and MSH.

STAR METHODS

Resource availability

Lead contact

Requests for fly lines, reagents, and additional questions should be directed to Dr. Andrea Page-McCaw (andrea.page-mccaw@vanderbilt.edu)

Materials availability

Fly lines generated in this study are available from the Bloomington Drosophila Stock Center or from the lead contact.

Data availability

All microscopy movies have been stored on Dropbox and can be made available for download upon request.

Experimental model and subject details

Drosophila melanogaster

Drosophila lines used in this study are in Table S1. Complete genotypes for each figure are available in Table S2. All *Drosophila* lines were maintained on standard cornmeal-molasses media supplemented with dry yeast. All flies, except those used in heat-shock flip clonal analysis, were raised at room temperature. For clonal analysis experiments flies were raised at 18 degrees Celsius until the 3rd instar stage when they were heat shocked in a circulating water bath at 37 degrees Celsius for 3 minutes. They were then allowed to develop at room temperature to 15-18hr after puparium formation (APF) before wounding experiments (described below) were conducted.

Method details

Pupal mounting

At room temperature, white prepupae were identified and marked within plastic food vials. Pupae were allowed to age until the 15-18 APF stage. 15-18 APF pupae were then removed from the vial onto a piece of double-sided tape (Scotch brand, catalogue #665) applied to a microscope slide. Using fine forceps, the anterior pupal case was removed exposing the head and notum of all pupae applied to the tape, as previously described in [29, 30]. The tape was carefully removed from the microscope slide and inverted onto a pre-prepared cover glass (Corning 2980-246, 24 mm x 64 mm) [31]. The pupae were carefully pressed down onto the cover glass by adhering the section of tape above the pupal head. Once the notum was visibly pressed onto the cover glass an oxygen permeable membrane (YSI, standard membrane kit, cat#1329882) was applied to prevent the pupae from drying out during imaging.

Pupal survival

Following imaging, pupae were kept mounted as described above and allowed to continue to develop and eclose for 3-4 days. Pupae that continued developing until they were able to crawl out of the partially dissected case were classified as ‘survived’ and their data acquired form these samples were used for analysis. If a pupae did not survive to eclosion, the associated datasets were not used in the study.

Live imaging

Images were collected using a Nikon Ti2 Eclipse with X-light V2 spinning disc (Nikon, Tokyo, Japan) with a 40X 1.3 NA oil-immersion objective or 60X 1.4 NA oil-immersion objective. Unless otherwise noted samples were imaged pre-wounding, immediately after wounding, every 2 min for 30 min, and then every 10 min for 6 hr. Images were pre-processed in NIS-Elements using combinations of background subtraction, rolling ball correction, local contrast, and

Denoise a.i. Assembly of figure panels was done using Affinity Designer and frames were centered on the entity in focus, compensating for frame shift due to wounding.

Laser ablation

A single pulse of a 3rd harmonic (355 nm) Q-switched Nd:YAG laser (5 ns pulse-width, Continuum Minilite II, Santa Clara, CA) was used for laser ablation. Laser pulse energies were kept to 1.9 μJ +/- 0.1 μJ, increased from our previously report [32] to keep the wound size similar between old and new ablation rig.

Border breakdown and tangential vs radial assignment analysis

Individual border breakdown events were manually observed using FIJI by identifying syncytia late in the movie and back-tracking to determine which borders broke down to form them. Each border that was broken down was traced back to the first frame after wounding to develop the map on Fig 1G. For each border breakdown, distance from the center of the wound and time after wounding were recorded in Microsoft excel. Border breakdown events were categorized as tangential or radial based on the orientation of the border relative to a vector pointing outward from the center of the wound. Specifically, the line tool in FIJI was used to measure both the angle of the border with respect to the horizon, theta, and the angle of the line from the center of the wound to the center of the border with respect to the horizon, alpha. If cos(alpha-theta) was less than cos(45 degrees), then the border was classified as tangential. Otherwise, the border was classified as radial.

Shrinking cell initiation / duration analysis

Shrinking cells were identified in live microscopy movies by beginning at the end of the movie and playing backwards in FIJI. Backwards, a shrinking cell appears to bloom from the epithelial layer, characterized by the expansion of a bright puncta of P120ctnRFP. Each cell that underwent

this behavior was marked on a single frame of the movie, then the distance from the center of the wound when shrinking started was denoted as well as the time that the shrinking started and completed. All cells that shrank were then manually traced back to the first frame after wounding to develop the map of shrinking cells (Fig 2C).

Approximating nuclei per syncytia

Nuclei and cell borders do not align in Z-projections of the pupal notum as the cells are non-prismatic. To estimate the number of nuclei per syncytium, the pre-wounding density of nuclei per unit area was determined for the circular region where syncytia form after wounding. Next, the apical area of the three largest syncytia/cells around a wound was measured at 0h, 1 hr and 2 hr post wounding. The area of each syncytia was multiplied by the nuclear density to yield the approximate number of nuclei per syncytia. The number of nuclei in each of the three syncytia was averaged to give a value for each of three samples in Fig. 1B.

Measuring apical area of syncytia across varied wound sizes

The three largest syncytia were determined by eye in FIJI for six samples, three ablated at 1.5 µJ and three ablated at 3 µJ ablation. The apical area of syncytia was measured 3 hr post wounding using the p120ctnRFP signal. Initial wound size was calculated by measuring Myosin II marked leading edge when it became apparent 30-160 min post wounding.

Unfused cells at leading edge: count and percent analysis

Unfused cells at the leading edge were identified using FIJI by a lack of border breakdowns. Each unfused cell was manually observed over the duration of wound closure and the time at which it departed from the leading edge was noted. A count of unfused cells at the leading edge was created in Excel and formal graphs were generated using Prism 9. To measure percent of the leading edge comprised of unfused vs. syncytial cells, each unfused cell's leading edge contact

was measured in FIJI using the polygon line tool. The total circumference of the wound was measured using the polygon line tool and unfused cell measurements were subtracted from the total to infer the syncytial occupancy at the leading edge. Formal histograms were generated using Prism 9.

Analyzing GFP labeled cells

107 individually labeled GFP cells were analyzed across 5 wounds over 6.5 hr. The position of the ablation was optimized to place as many individually labeled cells within 40-80um from the center of the wound as possible. After wounding it was possible to identify a mixing event by the decrease in intensity from the source cell with a corresponding increase in intensity of a previously unlabeled neighbor. Intensity differences made it possible to distinguish instances where two source cells were adjacent to each other but only one had a mixing event. However, large patches of source cells were not evaluated because inter-patch mixing was not distinguishable. To evaluate if border breakdowns were preceded by mixing, the 11 individually labeled cells that had border breakdowns were tracked back to the start of the movie and confirmed to have a mixing event. There was never an instance where a labeled source cell had a border breakdown without a prior mixing event occurring.

Wound Closure Analysis

A pigmented scar forms at the site of laser ablation making identifying the exact moment a wound is closed difficult. Since the scar is approximately the same size in each sample, the time point at which the Myosin II signal disappeared below the scar was used as a proxy for closure.

Calculating Intercalation

The change in the number of cells when the leading edge forms at 30 min (N_{start}) to when the wound is closed (N_{end}) is equal to the number of intercalations plus the number of radial fusion

events. Thus, (intercalations = ΔN – radial fusions). For the same three samples used in Fig 3D, we determined ΔN from N_{start} at 30 min and N_{end} when the wound had closed. Radial fusions were tallied by manually observing border breakdown events between the leading-edge cells and intercalations were calculated. Each radial fusion was counted as one prevented intercalation event.

REFERENCES

1. Cao, J., Wang, J., Jackman, C.P., Cox, A.H., Trembley, M.A., Balowski, J.J., Cox, B.D., De Simone, A., Dickson, A.L., Di Talia, S., et al. (2017). Tension Creates an Endoreplication Wavefront that Leads Regeneration of Epicardial Tissue. Dev Cell *42*, 600-615.e604.
2. Park, S., Gonzalez, D.G., Guirao, B., Boucher, J.D., Cockburn, K., Marsh, E.D., Mesa, K.R., Brown, S., Rompolas, P., Haberman, A.M., et al. (2017). Tissue-scale coordination of cellular behaviour promotes epidermal wound repair in live mice. Nat Cell Biol *19*, 155-163.
3. Galko, M.J., and Krasnow, M.A. (2004). Cellular and Genetic Analysis of Wound Healing in Drosophila Larvae. PLoS Biol *2*, e239.
4. Losick, V.P., Fox, D.T., and Spradling, A.C. (2013). Polyploidization and cell fusion contribute to wound healing in the adult Drosophila epithelium. Curr Biol *23*, 2224-2232.
5. Liu, Z., Yue, S., Chen, X., Kubin, T., and Braun, T. (2010). Regulation of cardiomyocyte polyploidy and multinucleation by CyclinG1. Circ Res *106*, 1498-1506.
6. Davies, P.S., Powell, A.E., Swain, J.R., and Wong, M.H. (2009). Inflammation and Proliferation Act Together to Mediate Intestinal Cell Fusion. PloS one *4*, e6530.
7. Alvarez-Dolado, M., Pardal, R., Garcia-Verdugo, J.M., Fike, J.R., Lee, H.O., Pfeffer, K., Lois, C., Morrison, S.J., and Alvarez-Buylla, A. (2003). Fusion of bone-marrow-derived cells with Purkinje neurons, cardiomyocytes and hepatocytes. Nature *425*, 968-973.
8. Corbel, S.Y., Lee, A., Yi, L., Duenas, J., Brazelton, T.R., Blau, H.M., and Rossi, F.M. (2003). Contribution of hematopoietic stem cells to skeletal muscle. Nat Med *9*, 1528-1532.
9. Nygren, J.M., Jovinge, S., Breitbach, M., Säwén, P., Röll, W., Hescheler, J., Taneera, J., Fleischmann, B.K., and Jacobsen, S.E. (2004). Bone marrow-derived hematopoietic cells generate cardiomyocytes at a low frequency through cell fusion, but not transdifferentiation. Nat Med *10*, 494-501.
10. Al-Maawi, S., Orlowska, A., Sader, R., James Kirkpatrick, C., and Ghanaati, S. (2017). In vivo cellular reactions to different biomaterials-Physiological and pathological aspects and their consequences. Semin Immunol *29*, 49-61.
11. Guirao, B., Rigaud, S.U., Bosveld, F., Bailles, A., López-Gay, J., Ishihara, S., Sugimura, K., Graner, F., and Bellaïche, Y. (2015). Unified quantitative characterization of epithelial tissue development. eLife *4*, e08519.
12. Ogura, Y., Wen, F.-L., Sami, M.M., Shibata, T., and Hayashi, S. (2018). A Switch-like Activation Relay of EGFR-ERK Signaling Regulates a Wave of Cellular Contractility for Epithelial Invagination. Developmental Cell *46*, 162-172.e165.

13. Tetley, R.J., Staddon, M.F., Heller, D., Hoppe, A., Banerjee, S., and Mao, Y. (2019). Tissue Fluidity Promotes Epithelial Wound Healing. Nat Phys *15*, 1195-1203.
14. Kakanj, P., Bhide, S., Moussian, B., and Leptin, M. (2022). Autophagy–mediated plasma membrane removal promotes the formation of epithelial syncytia. The EMBO Journal *41*, e109992.
15. Kim, J.H., Jin, P., Duan, R., and Chen, E.H. (2015). Mechanisms of myoblast fusion during muscle development. Current opinion in genetics & development *32*, 162-170.
16. Lehka, L., and Rędowicz, M.J. (2020). Mechanisms regulating myoblast fusion: A multilevel interplay. Seminars in Cell & Developmental Biology *104*, 81-92.
17. Wang, Y., Antunes, M., Anderson, A.E., Kadrmas, J.L., Jacinto, A., and Galko, M.J. (2015). Integrin Adhesions Suppress Syncytium Formation in the Drosophila Larval Epidermis. Curr Biol *25*, 2215-2227.
18. Renaud, S.J., and Jeyarajah, M.J. (2022). How trophoblasts fuse: an in-depth look into placental syncytiotrophoblast formation. Cellular and Molecular Life Sciences *79*, 433.
19. Søe, K. (2020). Osteoclast Fusion: Physiological Regulation of Multinucleation through Heterogeneity-Potential Implications for Drug Sensitivity. Int J Mol Sci *21*.
20. Leroy, H., Han, M., Woottum, M., Bracq, L., Bouchet, J., Xie, M., and Benichou, S. (2020). Virus-Mediated Cell-Cell Fusion. Int J Mol Sci *21*.
21. Pawelek, J.M., and Chakraborty, A.K. (2008). Fusion of tumour cells with bone marrow-derived cells: a unifying explanation for metastasis. Nature Reviews Cancer *8*, 377-386.
22. Wang, Y., Wang, Y., and Zheng, W. (2013). Cytologic changes of ovarian epithelial cancer induced by neoadjuvant chemotherapy. Int J Clin Exp Pathol *6*, 2121-2128.
23. Illidge, T.M., Cragg, M.S., Fringes, B., Olive, P., and Erenpreisa, J.A. (2000). Polyploid giant cells provide a survival mechanism for p53 mutant cells after DNA damage. Cell Biol Int *24*, 621-633.
24. Ogden, A., Rida, P.C.G., Knudsen, B.S., Kucuk, O., and Aneja, R. (2015). Docetaxel-induced polyploidization may underlie chemoresistance and disease relapse. Cancer Letters *367*, 89-92.
25. Mosieniak, G., Sliwinska, M.A., Alster, O., Strzeszewska, A., Sunderland, P., Piechota, M., Was, H., and Sikora, E. (2015). Polyploidy Formation in Doxorubicin-Treated Cancer Cells Can Favor Escape from Senescence. Neoplasia *17*, 882-893.
26. Zhao, Q., Zhang, K., Li, Z., Zhang, H., Fu, F., Fu, J., Zheng, M., and Zhang, S. (2021). High Migration and Invasion Ability of PGCCs and Their Daughter Cells Associated With the Nuclear Localization of S100A10 Modified by SUMOylation. Front Cell Dev Biol *9*, 696871.
27. Qu, Y., Zhang, L., Rong, Z., He, T., and Zhang, S. (2013). Number of glioma polyploid giant cancer cells (PGCCs) associated with vasculogenic mimicry formation and tumor grade in human glioma. J Exp Clin Cancer Res *32*, 75.
28. Weihua, Z., Lin, Q., Ramoth, A.J., Fan, D., and Fidler, I.J. (2011). Formation of solid tumors by a single multinucleated cancer cell. Cancer *117*, 4092-4099.
29. James T. O'Connor, E.K.S., M. Shane Hutson, Andrea Page-McCaw (In revision at STAR Protocols). Mounting Drosophila pupae for laser ablation and live imaging of the dorsal thorax. STAR Protocols.
30. Shannon, E.K., Stevens, A., Edrington, W., Zhao, Y., Jayasinghe, A.K., Page-McCaw, A., and Hutson, M.S. (2017). Multiple Mechanisms Drive Calcium Signal Dynamics around Laser-Induced Epithelial Wounds. Biophys J *113*, 1623-1635.
31. O'Connor, J.T., Shannon, E.K., Hutson, M.S., and Page-McCaw, A. (2022). Mounting Drosophila pupae for laser ablation and live imaging of the dorsal thorax. STAR Protoc *3*, 101396.
32. O'Connor, J.T., Stevens, A.C., Shannon, E.K., Akbar, F.B., LaFever, K.S., Narayanan, N.P., Gailey, C.D., Hutson, M.S., and Page-McCaw, A. (2021). Proteolytic activation of Growth-blocking

peptides triggers calcium responses through the GPCR Mthl10 during epithelial wound detection. Dev Cell *56*, 2160-2175.e2165.

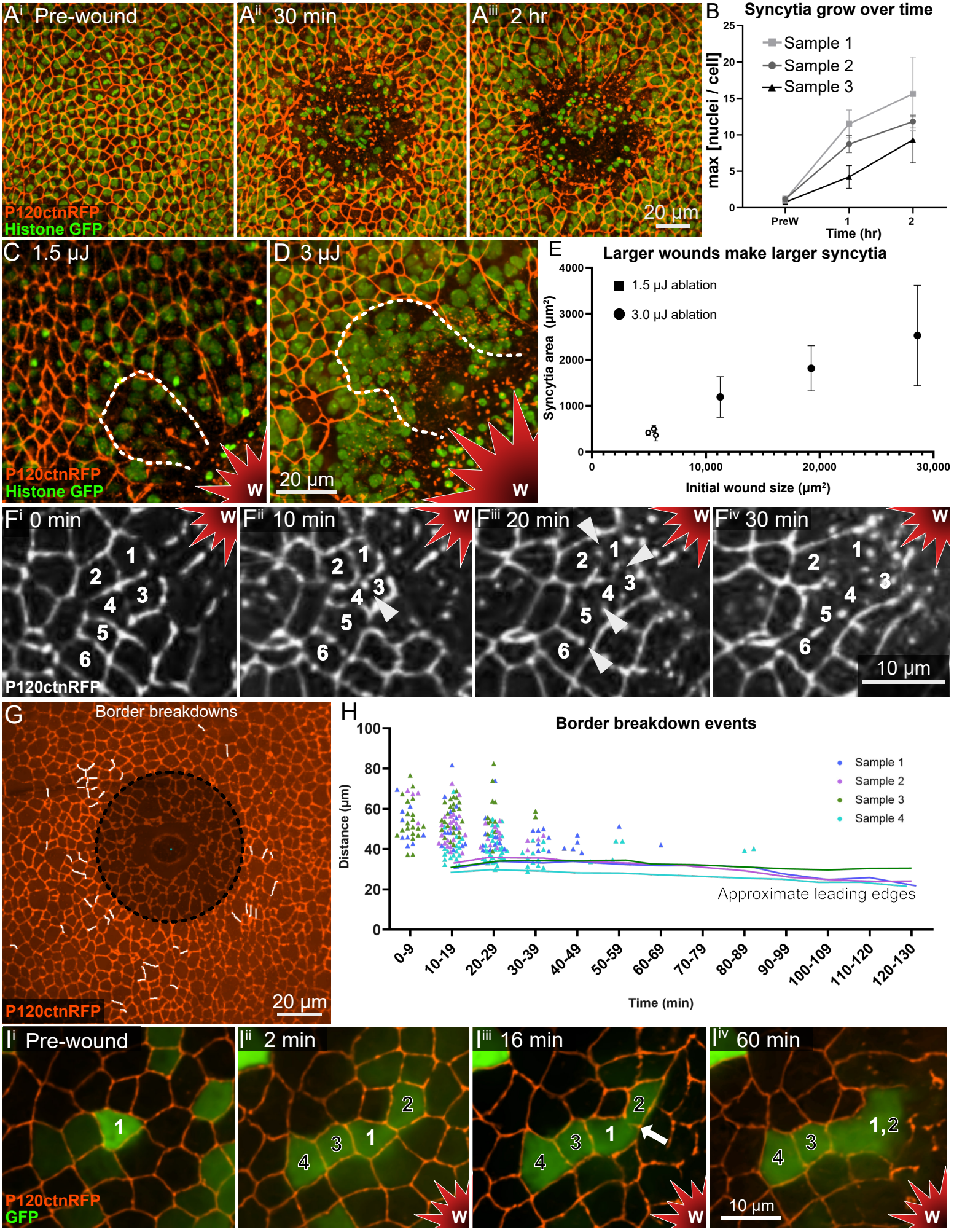
Ai Pre-wound
Aii 30 min
Aiii 2 hr
P120ctnRFP
Histone GFP
20 µm
B
Syncytia grow over time
Sample 1
Sample 2
Sample 3
max [nuclei / cell]
Time (hr)
PreW
C 1.5 µJ
D 3 µJ
W
E
Larger wounds make larger syncytia
1.5 µJ ablation
3.0 µJ ablation
Syncytia area (µm²)
Initial wound size (µm²)
Fi 0 min
Fii 10 min
Fiii 20 min
Fiv 30 min
10 µm
G
Border breakdowns
H
Border breakdown events
Sample 1
Sample 2
Sample 3
Sample 4
Distance (µm)
Approximate leading edges
Time (min)
Ii Pre-wound
Iii 2 min
Iii 16 min
Iiv 60 min
GFP

FIG 1

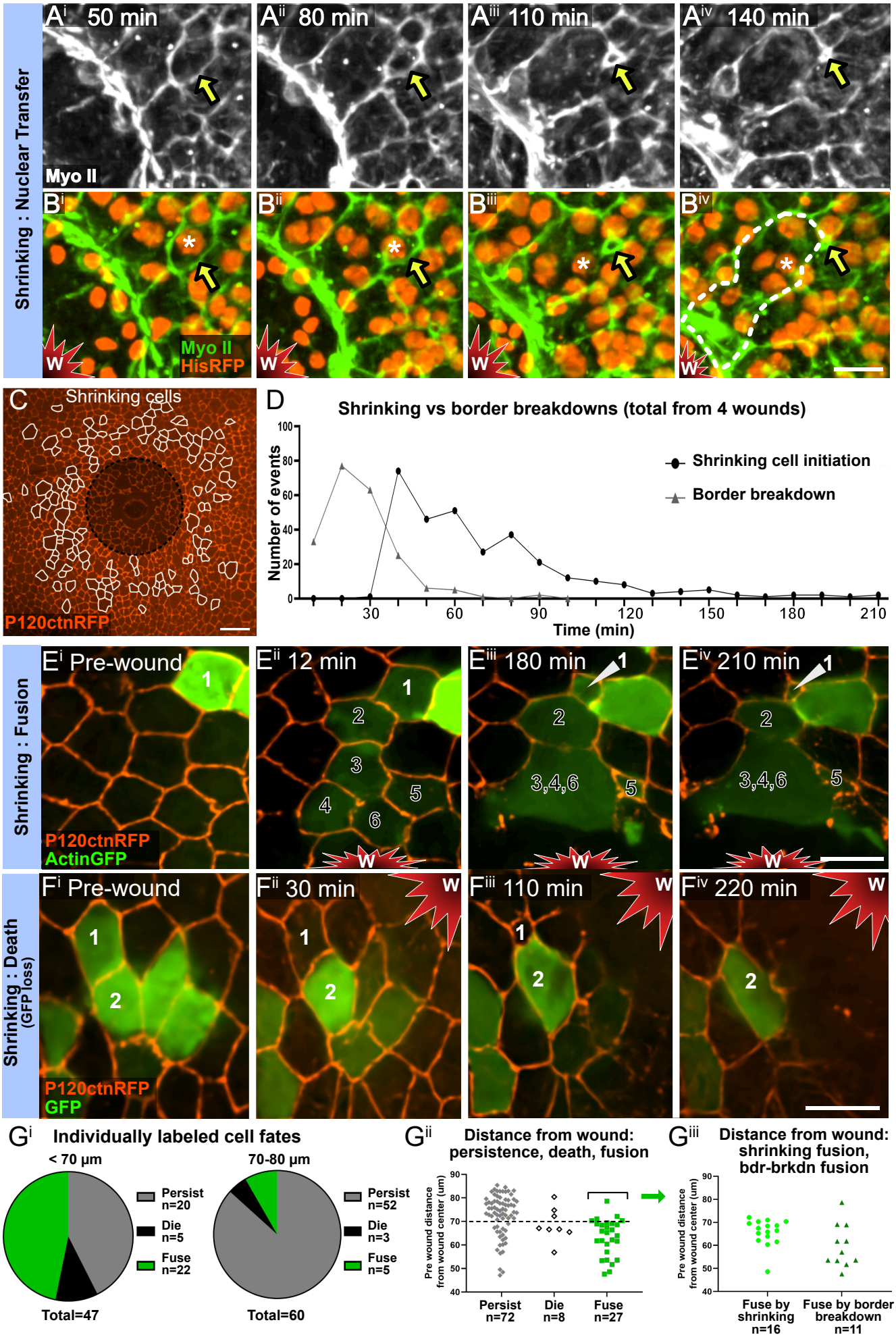
Shrinking : Nuclear Transfer
Ai 50 min
Aii 80 min
Aiii 110 min
Aiv 140 min
Myo II
Bi
Bii
Biii
Biv
Myo II
HisRFP
W
C
Shrinking cells
P120ctnRFP
D
Shrinking vs border breakdowns (total from 4 wounds)
Number of events
Time (min)
Shrinking cell initiation
Border breakdown
Shrinking : Fusion
Ei Pre-wound
Eii 12 min
Eiii 180 min
Eiv 210 min
P120ctnRFP
ActinGFP
Shrinking : Death
(GFP loss)
Fi Pre-wound
Fii 30 min
Fiii 110 min
Fiv 220 min
P120ctnRFP
GFP
Gi Individually labeled cell fates
< 70 µm
Persist n=20
Die n=5
Fuse n=22
Total=47
70-80 µm
Persist n=52
Die n=3
Fuse n=5
Total=60
Gii Distance from wound: persistence, death, fusion
Pre wound distance from wound center (um)
Persist n=72
Die n=8
Fuse n=27
Giii Distance from wound: shrinking fusion, bdr-brkdn fusion
Fuse by shrinking n=16
Fuse by border breakdown n=11

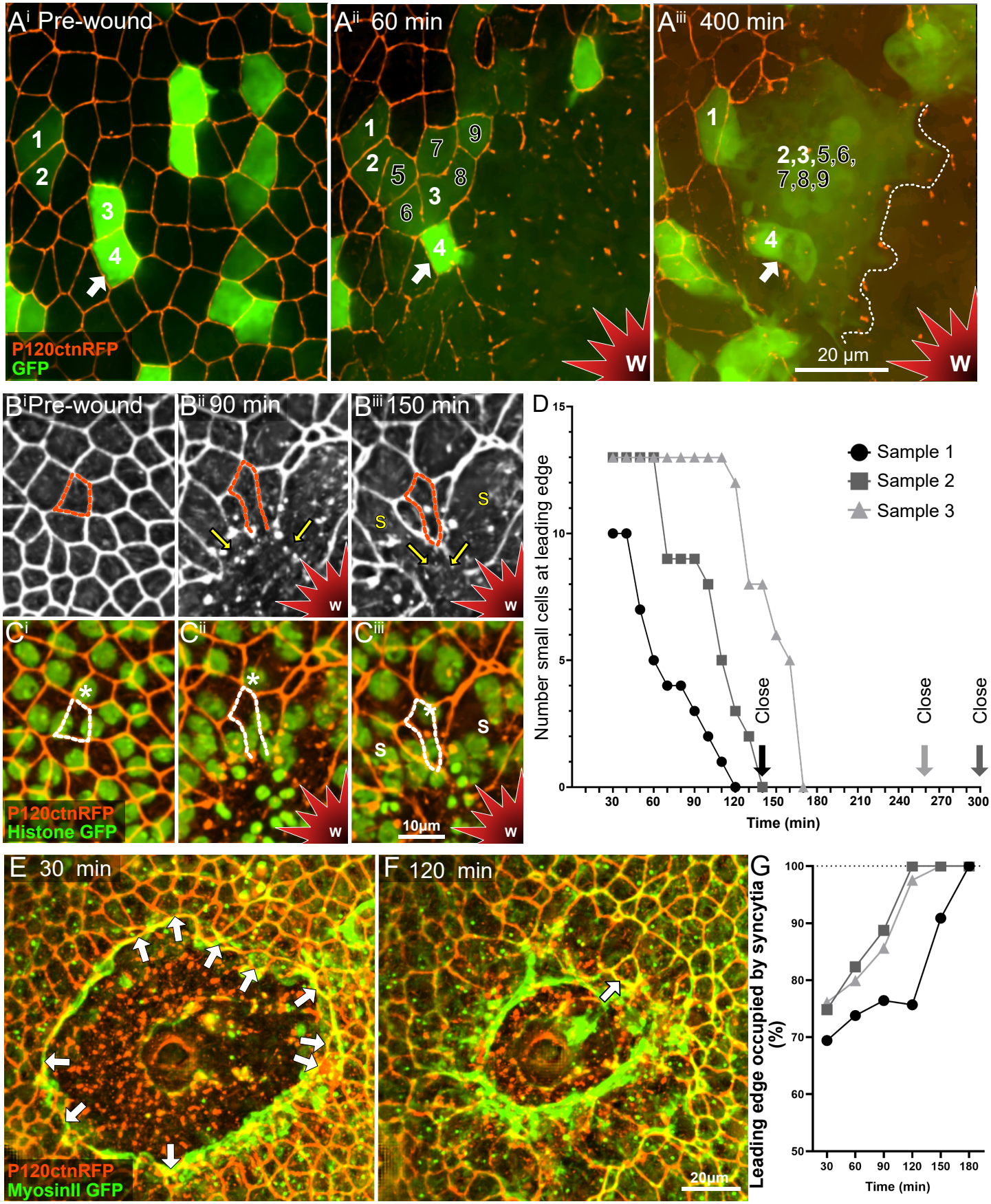
A^i Pre-wound
A^ii 60 min
A^iii 400 min
1
2
3
4
5
6
7
8
9
2,3,5,6,
7,8,9
20 µm
W
P120ctnRFP
GFP
B^i Pre-wound
B^ii 90 min
B^iii 150 min
S
C^i
C^ii
C^iii
P120ctnRFP
Histone GFP
10µm
D
Number small cells at leading edge
Time (min)
Sample 1
Sample 2
Sample 3
Close
E 30 min
F 120 min
P120ctnRFP
MyosinII GFP
20µm
G
Leading edge occupied by syncytia (%)
Time (min)

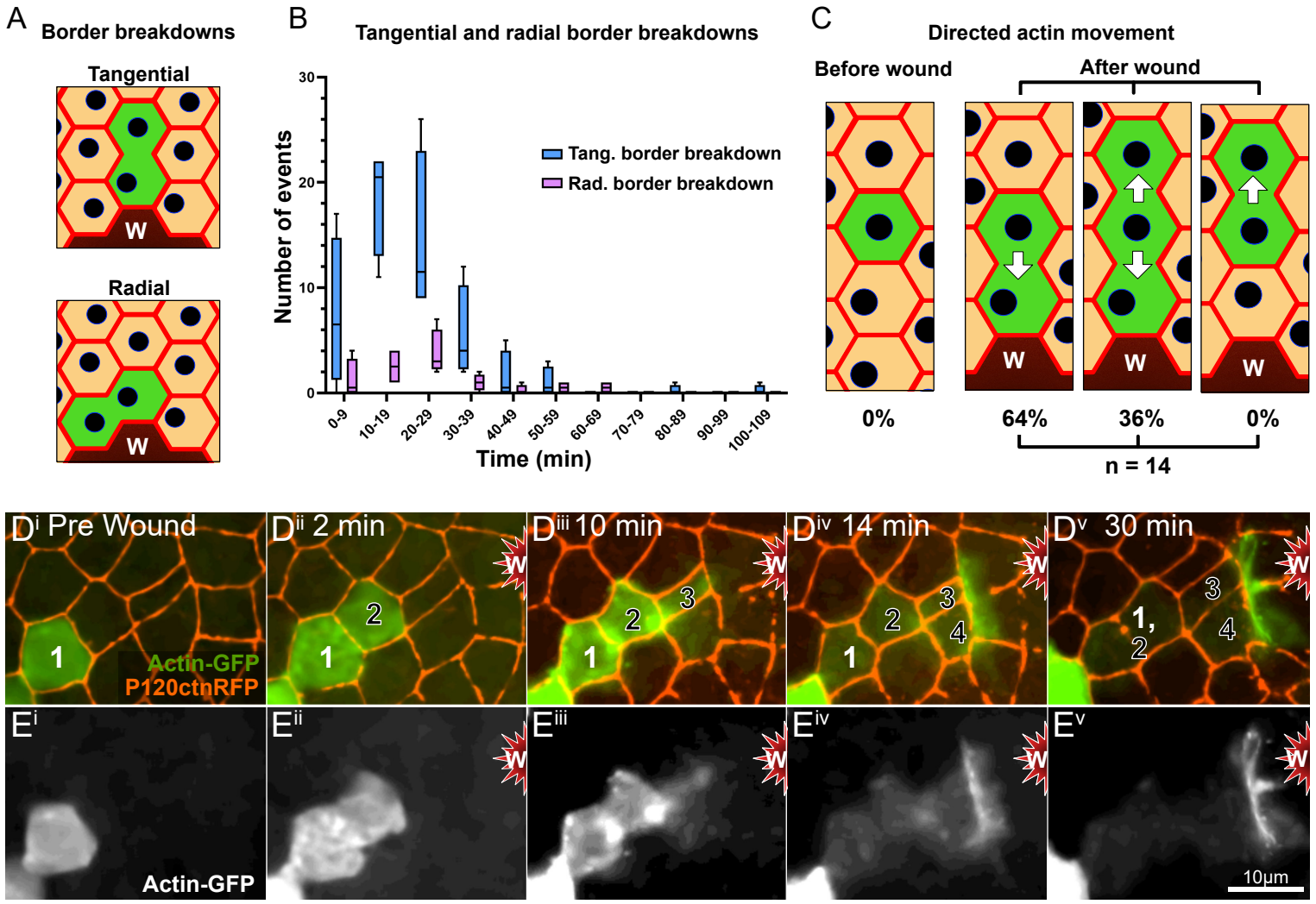

F

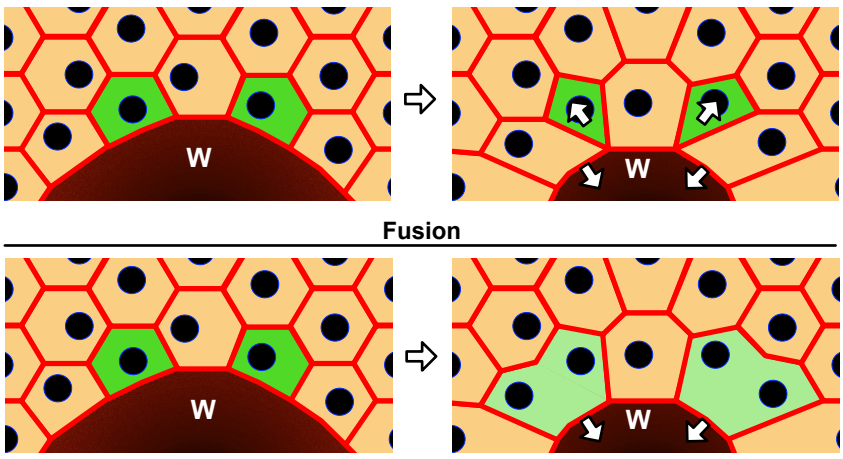

G

sample no.	Δ cells at leading edge	fusions	intercalations	% intercalations eliminated by fusions	Time of closure
1	39	16	23	41%	140 min
2	42	7	35	17%	300 min
3	43	15	28	35%	260 min

Key resources table

REAGENT or RESOURCE	SOURCE	IDENTIFIER
Antibodies		
Bacterial and virus strains		
Biological samples		
Chemicals, peptides, and recombinant proteins		
Critical commercial assays		
Deposited data		
Experimental models: Cell lines		
Experimental models: Organisms/strains		

See Table S1	Various	N.A.
Oligonucleotides		
Recombinant DNA		
Software and algorithms		
FIJI	Schindelin et al., 2012	RRID: SCR_002285
NIS Elements	Nikon Instruments Inc.	RRID: SCR_014329
Microsoft Excel	Microsoft	https://www.microsoft.com/en-us/microsoft-365/excel
GraphPad Prism 9	GraphPad	https://www.graphpad.com/scientific-software/prism/
Affinity Designer	Affinity Serif	https://affinity.serif.com/en-us/designer/
Other		